Assessing Last-Mile Space–Time Accessibility with Barriers via Generative Navigational Agents

Beyza Kurtulmus*[1], Feixiong Liao[2]

[1] PhD Candidate, Department of Built Environment, Yildiz Technical University, Turkey.

[2] Assoc. Prof. Dr., Eindhoven University of Technology, the Netherlands.

SHORT SUMMARY

Conventional last-mile accessibility assessments often assume isotropic motion, neglecting the impact of physical barriers and cognitive pathfinding on accessibility. This research investigates the last-mile mobility by assessing how urban barriers and frictions disrupt last-mile accessibility. The study presents a hybrid framework integrating high-resolution LiDAR data with large language modeling (LLM). LiDAR data locates barriers and measures barrier impedance, while LLMs serve as generative navigational agents to simulate barrier-adaptive decision-making. This two-tiered methodology transforms unprocessed spatial limitations into accessibility metrics within space-time prisms. Findings based on two comparative case studies reveal that conventional models omitting physical barriers have significant accessibility overestimations, which advocates for human-centered designs in non-idealized urban areas.

Keywords: accessibility, last-mile mobility, LiDAR point clouds technology, large language modeling, space-time prism, urban morphology.

1. INTRODUCTION

Urban mobility is influenced by the interaction between temporal constraints and spatial opportunities. In time-geography, the space–time prism (STP) is the theoretical construct for mapping human mobility boundaries (Hägerstrand, 1970). While traditional STP models often treat urban space as a frictionless, isotropic plane, actual movement is dictated by the physical complexities of the built environment. In multimodal travel chains, the first-mile typically benefits from residential familiarity and feeder network integration; however, the last-mile stage represents the most vulnerable segment where pedestrians may encounter high-density morphological fragmentations (Tokey et al., 2025). Existing frameworks struggle to account for this urban resistance, where physical barriers impose severe constraints on mobility boundaries, detrimental to the accuracy of last-mile accessibility assessments. Current literature frequently performs assessments based on Euclidean distance divided by average speed, establishing an idealized theoretical baseline. Yet, navigating the physical environment exceeds these idealized projections. Despite the recognition that last-mile efficiency affects overall travel choices (Liao et al., 2020), most models overlook physical impediments, resulting in accessibility overestimations of up to 38% (Udhayasekar et al., 2026). Pedestrians endure considerable time costs to bypass unfavorable settings, highlighting the need for models that prioritize urban friction over idealized representations (Tong and Bode, 2022).

In the last-mile area with barriers, accessibility is not a predetermined outcome but a process of active spatial learning and real-time adaptation. Traditional simulation-based models lack the granularity to represent the cognitive flexibility required to bypass fragmented landscapes (Tong and Bode, 2022). While reinforcement learning (RL) and agent-based modeling (ABM) are widely utilized, they struggle to accommodate the human-like spatial reasoning necessary for such adaptation in non-routine navigations (Gershman & Daw, 2017; He et al., 2022) Furthermore, despite the potential of large language models (LLMs) as dynamic navigational engines capable of real-time learning, current literature predominantly utilizes them as 'fixed predictors' for travel choice rather than operationalizing

spatial reasoning (Argyle et al., 2023). These represent a critical research gap in urban mobility modeling: existing frameworks fail to bridge the discrepancy between idealized reachability and actual temporal costs within the last-mile stage. This study investigates the extent to which physical barriers restrict last-mile accessibility and quantifies the degree to which traditional models overlook these constraints. The study proposes a last-mile modeling approach centered on STP efficiency, simulating a learning trajectory of a long time frame that conceptualizes the transition from high-uncertainty cognitive navigation to (near-)optimal routing by internalizing urban frictions into the prism's geometric boundaries.

To achieve this, the methodology integrates LiDAR point cloud data with LLM-driven generative navigational agents (GNAs). By locating physical barriers through LiDAR-derived height and flatness data, the framework replaces a static last-mile area with a high-resolution 3D representation. LLM-based spatial reasoning allows GNAs to autonomously refine trajectories by accounting for morphological resistance. Through a comparative evaluation of Amsterdam's Station Square and Istanbul's Beşiktaş Barbaros Square, the research illustrates how urban frictions affect last-mile accessibility. The remainder of this paper is organized as follows. Section 2 details the hybrid methodology; Section 3 presents the experimental results; and Section 4 discusses urban planning implications and future directions.

2. METHODOLOGY

The methodology integrates three modules: a morphological engine, a GNA cognitive loop, and an empirical analysis. First, the morphological engine processes LiDAR data to locate physical barriers within a 3D voxelized environment. Second, the GNAs utilize an LLM-driven "Save-Reflect-Retrieve" cycle to transform physical barrier score inputs into subjective spatial knowledge. Finally, the framework employs inverse calibration against GPS clusters to quantify the STP efficiency ratio, providing the discrepancy between theoretical and realizable accessibility and mobility.

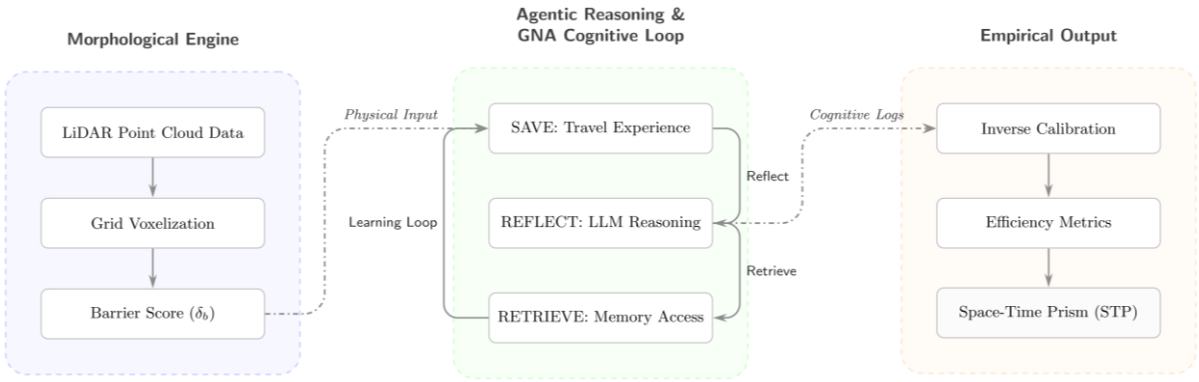


Figure 1: Research methodology.

Space-Time Prisms with Barriers

The study formalizes the potential path area (PPA) through three layers of environmental and cognitive complexity, within the last-mile area. The first layer, idealized PPA (PPA_{id}), serves as a frictionless baseline (Eq. (1)) based on Euclidean distance and fixed travel time. The second layer, barrier-adjusted PPA (PPA_{ba}), integrates physical barriers (Eq. (2)) via LiDAR data to calculate objectively measured travel time, accounting for a reduced speed (v_b) and temporal penalty δ_b. The final layer, realizable PPA (PPA_{re}), incorporates learnt mobility (Eq. (3)) to constrain agent reachability (Kwan and Schwanen, 2016). Urban friction is mediated by the cognitive reasoning of GNAs, where an adaptive learning factor $\eta_k \in [0,1]$ reflects how spatial experience transforms physical constraints into realizable trajectories in the third layer. As η_k increases, the agent's cognitive adaptation grows, thereby reducing

the perceived impact of barriers, whereas a lower η_k indicates limited spatial experience. The following equations define the mathematical basis for these three layers.

$$PPA_{id} = \left\{ j \in \Omega \;\middle|\; \left(\frac{d(h_0,j)}{v} \right) + d_a + \left(\frac{d(j,h_1)}{v} \right) \leq T_\beta \right\} \tag{1}$$

$$PPA_{ba} = \left\{ j \in \Omega \mid t^B(h_0,j) + d_a + t^B(j,h_1) \leq T_\beta \right\} \tag{2}$$

$$PPA_{re} = \left\{ j \in \Omega \;\middle|\; \frac{t^B(h_0,j)}{\eta_k} + d_a + \frac{t^B(j,h_1)}{\eta_k} \leq T_\beta \right\} \tag{3}$$

where $d(h_0,j)$ and $d(j,h_1)$ are Euclidean distances between two anchor points (h_0 and h_1) and $j \in \Omega$ as a potential intermediate location for secondary activities in the last-mile area; d_a is the minimum activity duration; h_0 is the origin node representing the start of the last-mile segment, and h_1 is the final destination node (e.g., workplace); $t^B(h_0,j)$ and $t^B(j,h_1)$ are the barrier-adjusted travel times, in which; T_β is the time budget for the entire last-mile mobility chain; and η_k is the agent learning coefficient.

LiDAR Data Processing and Hexagonal Grid Construction

To operationalize physical constraints, the framework identifies barrier locations using LiDAR point-cloud datasets, distinguishing passable surfaces through automated ground-object classification (Asvadi et al., 2016). Within this LiDAR environment, sudden Z-coordinate shifts and flatness metrics categorize morphological information into three distinct regions: passable, semi-passable, and impassable areas (Asvadi et al., 2016). This voxel-based evaluation quantifies the adjusted average walking speed v_b in an area with barriers in (Eq. (4-)).

$$v_b = \frac{v \cdot A_p}{A_t} \tag{4}$$

$$\delta_b = \frac{d}{v_b} - \frac{d}{v} \tag{5}$$

where v_b is the barrier-adjusted average walking speed; A_t is the total floor area; and A_p is the passable area. The ratio A_p/A_t represents the permeability of the urban frictions. δ_b is the incremental time delay given distance d in (Eq. (5)). To precisely measure v_b, the last-mile area is divided into uniform hexagonal cells across different resolutions (see Figure 2 for an example using a side length of 100 m).

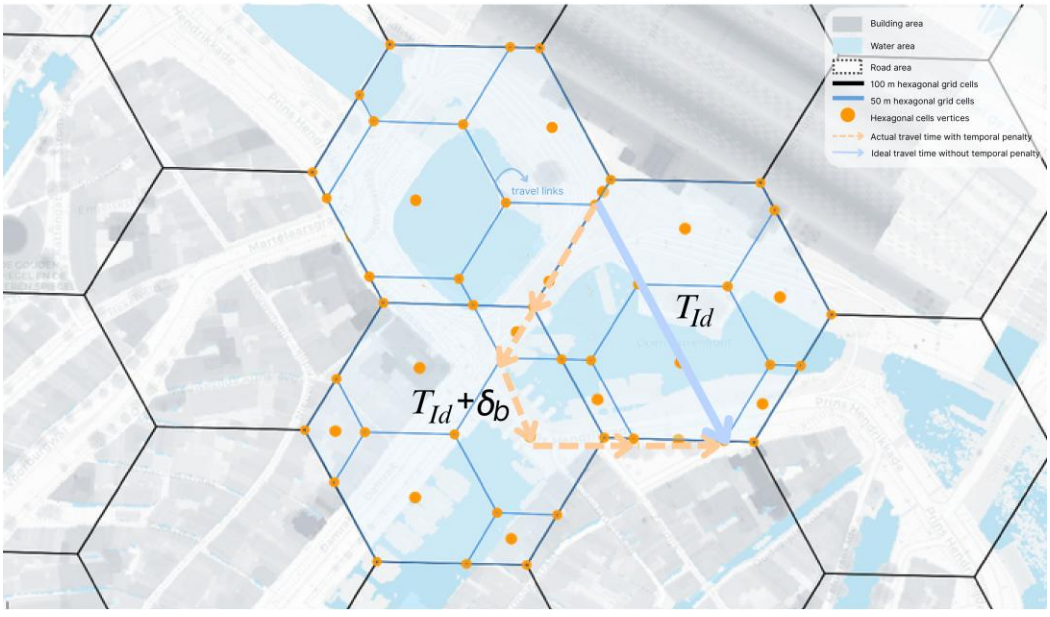


Figure 2: Hexagonal grid structure.

Utilizing multi-resolution hexagonal grids allows the framework to capture accessibility overestimations at various scales. Hexagonal cells minimize orientation bias in agent movement due to uniform neighboring distances. Within each cell represented as a unit network, the node set comprises the centroid, vertices, and edge midpoints, and the link set includes all the edges connecting the neighboring nodes. Therefore, each cell has a specific walking speed depending on the passable area. Given the side length of the cell, it is possible to calculate the walking time on every link associated with a cell and ultimately the entire last-mile area. As a consequence, $t^{\mathrm{B}}(h_0, j)$ and $t^{\mathrm{B}}(j, h_1)$ in Eq. (2) can be determined by performing standard shortest path searches.

Generative Navigational Agents (GNA): Integrating LLM Reasoning

The research utilizes GNAs to address the limitations of static algorithms in fragmented urban environments. While traditional models excel in static optimization, they struggle with high-level semantic reasoning in unfamiliar contexts (Chorus et al., 2024). The proposed GNA framework employs LLMs as a dynamic reasoning engine that interprets physical friction as a nuanced semantic signal. This architecture facilitates human-like spatial cognition by synthesizing an objective LiDAR-derived temporal penalty δ_b with long-term memory integration, effectively mimicking the heuristic shifts (Zhu et al., 2023).

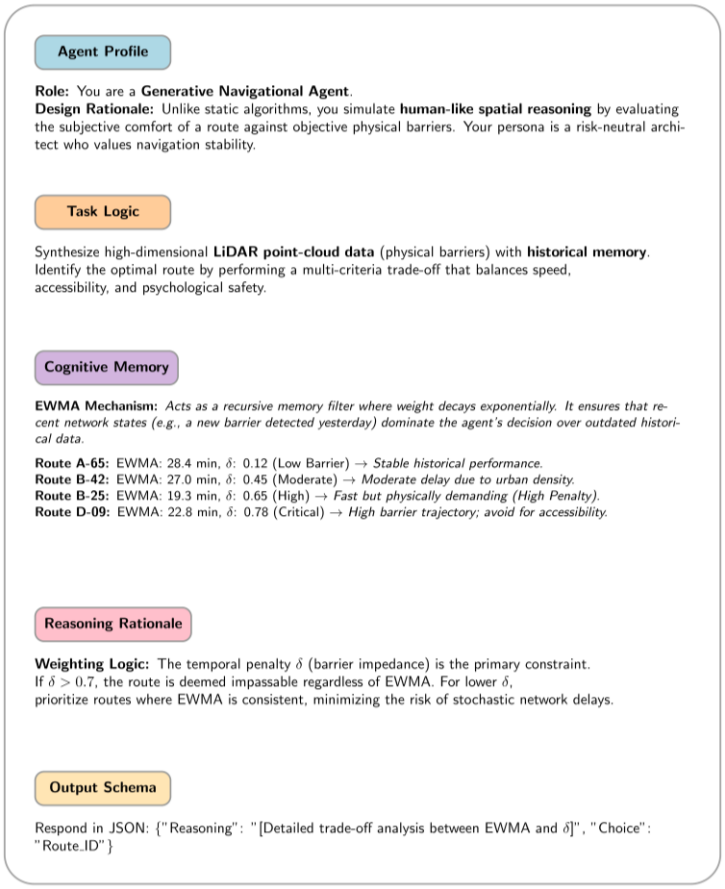


Figure 3: Structured GNA prompt.

Figure 3 illustrates this process through a structured prompt architecture consisting of four parts: (1) Profile, defining the agent's background and navigation persona; (2) Task, requiring the agent to optimize travel time by accounting for barrier impedance; (3) Memory, utilizing the experience weighted moving average (EWMA) as a recursive cognitive filter to prioritize recent experiences; and (4) Guidance, providing the strategic reasoning constraints. Employing EWMA, the model ensures that memory is a time-sensitive mechanism, allowing the LLM to navigate urban frictions through repeated interactions in the last-mile stage. GNAs follow a recursive learning cycle (Figure 4) governed by a

"Save-Reflect-Retrieve" loop to simulate spatial knowledge evolution. Assuming agents maintain reliable temporal records but operate under limited spatial certainty, they record daily durations and barrier encounters as perceptual input. The LLM reflects on this data to quantify friction by calculating the deviation from idealized travel times. This process updates spatial knowledge by adjusting the overall learning coefficient (η_k). Specifically, the LLM recalibrates η_k based on the ratio between perceived and objective friction; as η_k increases through repeated interactions, it scales down the impact of physical barriers t^{B} in the agent's decision-making process. Consequently, this feedback loop enables agents to autonomously re-optimize trajectories by prioritizing segments with lower perceived friction.

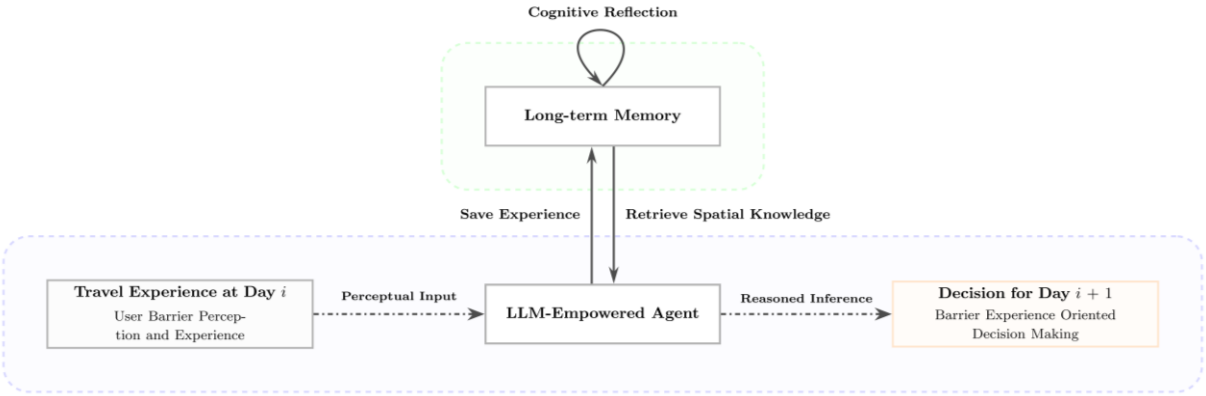


Figure 4: Recursive learning cycle.

Inverse Calibration and Empirical Verification

The GNA framework generates simulated trajectory sequences calibrated against empirical GPS data to update t^{B} and η_k. This process achieves a state of predictive alignment through the "Save-Reflect-Retrieve" cycle, where the agent's perceived friction converges with real-world travel times. To quantify the "reality gap", the framework utilizes two metrics: the temporal efficiency ratio (ΔT) serving as a direct proxy for space-time efficiency and the space-time accessibility index (E_{STA}), serving as a normalized ratio of the spatial distribution of opportunities within the potential path areas relative to the ideal baseline.

$$\Delta T = \frac{T_\beta - T_{re}}{T_\beta - T_{id}} \tag{6}$$

$$E_{STA} = \left(\frac{\sum_{j \in PPA_{re}} O_j}{\sum_{j \in PPA_{id}} O_j}\right) \tag{7}$$

where T_{id} is the frictionless Euclidean baseline; T_{re} incorporates the barrier-adjusted penalty (t^{B}) mediated by the agent's learning coefficient (n_k). As the agent reduces barrier impedance by cognitive adaptation, the spatial extent of the (PPA_{re}) expands; and PPA_{id} is the idealized PPA; O_j is related to the flexible activity opportunities (e.g., service points, retail locations)as formulated in Eq. (1–3). $\Delta T \rightarrow 1$ signifies a temporal efficiency gain through learning, , whereas $E_{STA} \leq 1$ represents the ratio of realized accessibility relative to the ideal potential, with values closer to 1 indicating (near-)optimal accessibility.

3. RESULTS AND DISCUSSION

Lidar-Derived Barrier Mapping and Morphological Characteristics



	Barrier Category	Height Range	Urban Element Examples	Impact on Accessibility
A	High-Level (Absolute)	$H \geq 1.5$ m	Facades, retaining/sound walls	Absolute obstruction; forces significant detours.
B	Mid-Level (Semi-Permeable)	$0.5 \text{ m} \leq H \leq 1.5$ m	Fences, guardrails, parked vehicles	Partial obstruction; increases cognitive/physical load.
C	Low-Level (Permeable)	$0.1 \text{ m} \leq H \leq 0.5$ m	Curbs, ledges, landscape borders	Minor effort; visually permeable; negligible route impact.
D	Environmental / Natural	Variable	Water bodies (canals), steep terrain	Natural barriers; movement restricted to specific points.

Figure 5: Study areas and barrier maps of Amsterdam (left) and Istanbul (right) cases.

The evaluation compares the regulated 17th-century canal-ring layout of Amsterdam Central Station Square with the fragmented fabric of Istanbul Beşiktaş Barbaros Square. These sites were selected for their analogous daily throughput (~400,000) and functional roles as multi-modal transportation hubs. High-resolution LiDAR (0.05 m) data quantifies urban constraints by classifying normalized height (H) based on pedestrian biomechanics and accessibility standards (ISO 21542, ADA). These thresholds reflect human walking constraints: ($0.1\ \text{m} \leq H \leq 0.5\ \text{m}$) for low-level, ($0.5\ \text{m} < H \leq 1.5\ \text{m}$) for mid-level, ($H > 1.5\ \text{m}$) for high-level, and environmental for natural parameters. These classes define the net passable area (A_p), within the total floor area (A_t) of a hexagon cell. 1000 generative agents ($v = 1.4\ \text{m/s}$) simulate movement from various h_0 (last-mile stage origin) and h_1 (destination) pairs at 10–60 minute thresholds, deriving the adjusted average velocity via (Eq. (4)) and the temporal penalty from the permeability ratio via (Eq. (5)). The operational impact is demonstrated through representative 100 m hexagonal cells A_t of 207.848 m^2 (A'_t=25.981 m^2 (total area for only one cell)) across Amsterdam Station Square. Within this extent, physical barriers restrict the cumulative passable area to 83.555 m^2. This 40.2% overall permeability ratio establishes a 1.67 scaling factor, which, from a bird's-eye perspective, effectively reduces the progression velocity from 1.4 m/s (v) to 0.84 m/s (v_b), representing a nearly two-fold slowdown in reaching the destination. The summation of reduced velocities results in a cumulative objective penalty of 381 s (6.3 minutes). This process shifts the ideal travel time from 571.4 s to 952 s (15.8 minutes). Conversely, the Beşiktaş Barbaros axis is more fragmented; absolute barrier impediments reduce A_p to 25.6%, leaving 74.4% of the surface nearly impassable. Such morphological resistance imposes substantial temporal penalties necessitating the adaptive navigation to account for systematic frictions omitted in isotropic accessibility frameworks.

Cognitive Adaptation, Learning Process, and η_k Evolution

The GNA decision logic (Table 1) provides the necessary context for convergence, as qualitative profiles are highly effective in shaping the quantitative evolution of travel adaptation. 30-day simulations track how agents minimize urban friction through continuous spatial learning. The heterogeneity of agent profiles, ranging from GPT 5.4 (IST) agents' preference for acoustic tranquillity to Llama-3 (AMS) agents' risk-seeking navigation, dictates the divergent temporal outcomes and learning trajectories observed by N = 30. To ensure these outcomes reflect real-world navigation, the framework bridges the gap between simulation and reality by calibrating agent behaviors against empirical GPS data from Amsterdam and Istanbul cases.

Table 1: Agent decision logic and spatial reasoning profiles.

Model & Site	Agent Profile & Key Traits	Choice Context & Memory	Logic / LLM Reasoning	Final Convergence Outcome
GPT-5.4 (AMS)	Bram (45–54, Architect) – Risk-neutral, Conscientious	Route choice under network volatility	Prioritizes structural consistency over short-term speed	Stable: Consistently chooses reliable, high-integrity routes
GPT-5.4 (IST)	Elif (65+, Retired) – Privacy-seeking, Introverted	Quiet vs. noisy route comparison	Prioritizes acoustic comfort; avoids high-decibel segments	Stable: Stabilizes on quiet, environmental-friendly paths
Llama-3 (AMS)	Amira (25–34, Boutique) – Risk-seeking, Neurotic	Fast-paced network navigation	Prioritizes exploration and speed to maximize gain	Variable: Shows frequent path switching and high exploration
Llama-3 (IST)	Bram (45–54, Architect) – Risk-neutral, Conscientious	Historical vs. real-time reliability	Favors long-term stability to ensure punctuality	Moderate: Balances historical data with current performance

Evaluating last-mile performance across 10m–100m grid resolutions identifies the 10m grid as the primary analysis unit. Figure 6 visualizes navigational intelligence evolution through the convergence of agent movement paths: At Day 1 ($n_k \approx 0$), "spatial ignorance" follows, with axis-bound trajectories

fragmented by topographical barriers and canals into disconnected clusters. By $N = 15$, the midpoint of cognitive calibration, the Save-Reflect-Retrieve loop begins bridging gaps through primary bypasses, though some redundancy remains. Finally, at Day 30 ($n_k \approx 1$), the network achieves "morphological fluency," where earlier sprawl contracts into a high-utility, consolidated envelope. The orange trajectories represent the emergent flow of successful agent passages, where the intensity of the color highlights the most efficient routes discovered to bypass urban impedances. This proves agents actively generate optimized routes rather than merely reacting to barriers, transforming raw impedance into a refined navigational grid. Consequently, the Day 1–30 transition illustrates the successful conversion of initial time losses into stabilized reach (E_{STA}). Other resolution dynamics are documented in the Appendix, Figures A1 and A2.

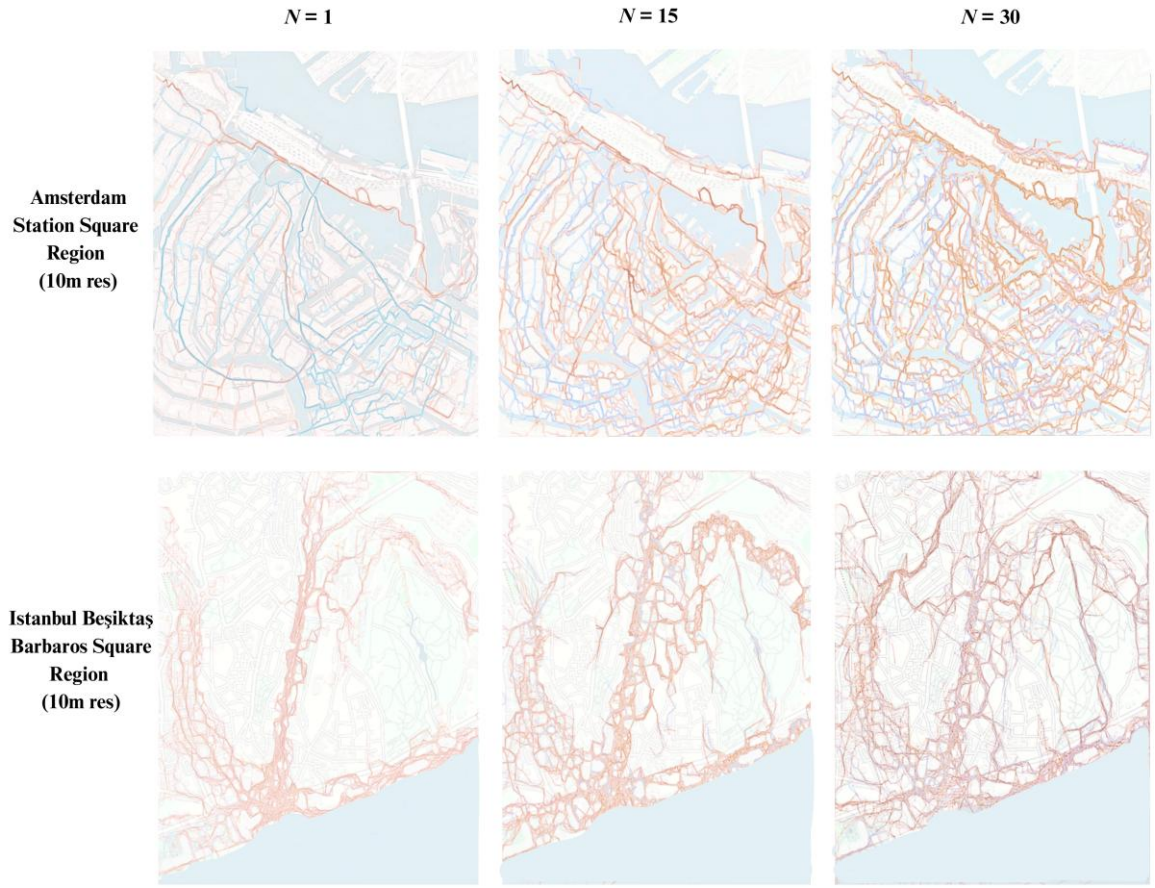


Figure 6: Geographic network simulations by 10 mgrid cellular structures

Figure 7 reveals a performance divergence. Istanbul Beşiktaş's fragmented morphology causes a higher cognitive demand as η_k curves stabilize near the 0.65-0.70 band, while Amsterdam Station Square stabilizes near 1.0, allowing for faster adaptation. Fragmented fabrics, thus, require greater cognitive adaptation to overcome spatial frictions. Regarding temporal convergence, both sites stabilize within 30 days despite differing trajectories. Beşiktaş starts at high latency (~50 min), dropping to 25 minutes as spatial learning mitigates initial network unfamiliarity. Conversely, Amsterdam's begins lower (~30 min) and settles below 18 minutes, confirming a less restrictive barrier threshold. By day 30, the increased trajectory density signifies consolidated (near-)optimal paths as agents transition from cognitive exploration to the repetitive utilization of optimized spatial routes.

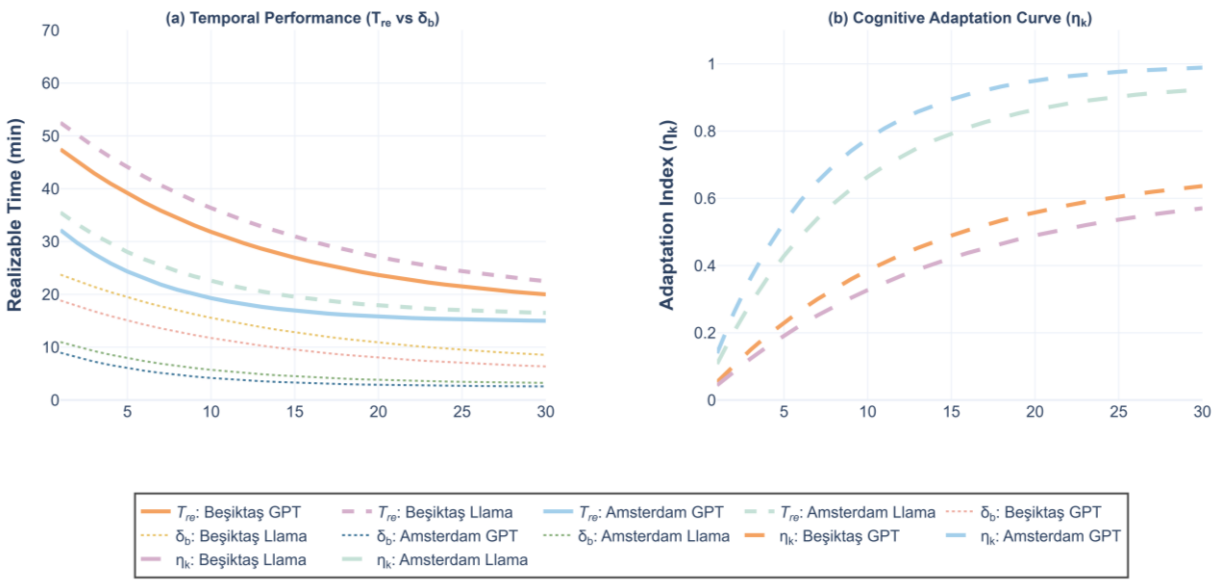


Figure 7: Multivariate relationship between the variables of τ_{re}, η_k, and δ_b

Comparative STP Efficiency Metrics

Comparative PPA analysis reveals how temporal penalty scales last-mile accessibility through STP efficiency. Figure 8 illustrates that Amsterdam Station Square's canals act as constraints, yet (PPA_{ba}) (Baseline) remains high at 82% of its (PPA_{id}) (Ideal). This allows a high $\Delta T \approx 0.915$ to recover significant movement potential, ensuring urban opportunities remain accessible despite barriers. Station Square maintains a PPA_{re} reach that equates to E_{STA} of 0.75, limiting total accessibility loss to 25%. Conversely, Istanbul Beşiktaş faces a higher accessibility loss; its PPA_{ba} starts at a restrictive 66%, limiting ΔT to 0.83. Despite adaptive navigation to optimize the travel time, the PPA_{re} reach only results in an E_{STA} of 0.55. Istanbul's fragmentation causes a more reduction in potential reach, nearly doubling Amsterdam's accessibility loss.

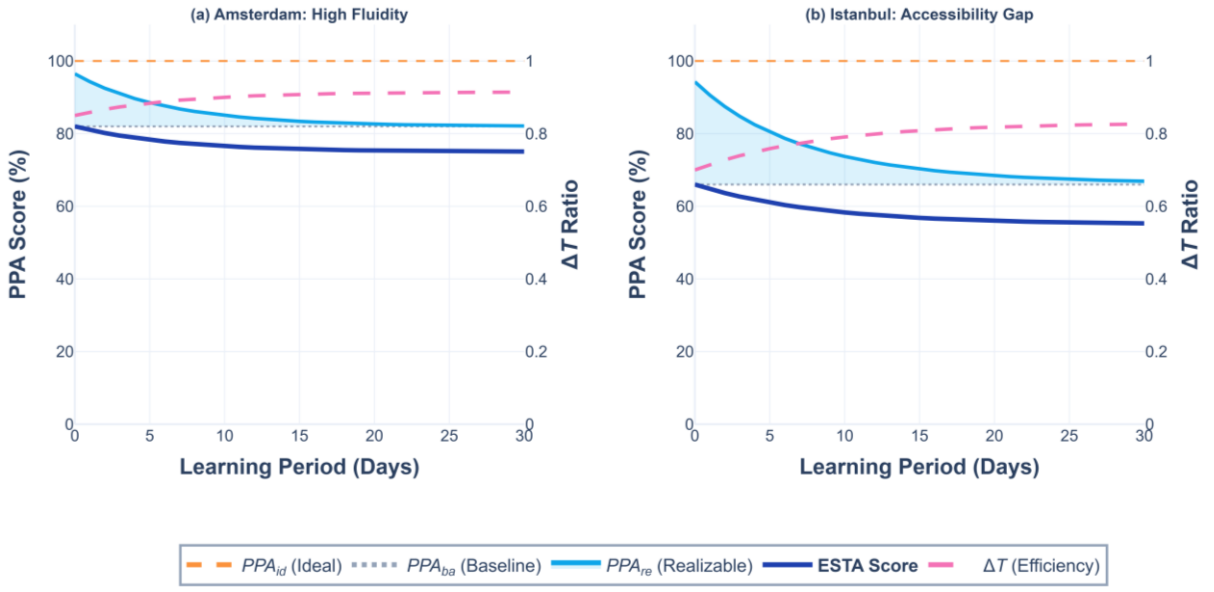


Figure 8: ΔT, STA, and PPA analysis graphs

The comparison validates the GNA model, showing how spatial configurations dictate last-mile accessibility. In Amsterdam Central Station Square, high permeability and legible transit structures minimize accessibility loss to 25%. Conversely, Istanbul Beşiktaş Barbaros Square exhibits a

fragmented fabric with severe topographical barriers, causing a 45% reduction in reach. These results confirm that while cognitive adaptation informs mobility, physical constraints remain the primary determinant of accessing urban destinations.

4. CONCLUSIONS

This study evaluates last-mile accessibility by integrating high-resolution LiDAR with LLM simulations in areas with barriers. The primary contribution is a hybrid framework merging barrier-adjusted STP with agent cognitive reasoning, quantifying accessibility as a synthesis of geometry and cognitive navigation. The GNA framework identifies high-friction zones where physical obstacles trigger iterative route adaptations. The case studies demonstrate that fragmented urban configurations impose significantly higher cognitive and temporal burdens, nearly double compared to integrated grids. These findings suggest that perceived accessibility is a dynamic function of spatial impedance and experience, rather than a static proximity metric. This generalization underscores the necessity for urban models to transition from isotropic assumptions to path-specific simulations. Ultimately, the observed correlation between agent exploration and efficiency calls for the future integration of subjective priorities and diverse pedestrian profiles into last-mile accessibility assessment.

REFERENCES

Argyle, L. P., Busby, E., Fulda, N., Gubler, J. R., Rytting, C., & Wingate, D. [2023]. Out of one, many: Using language models to simulate human samples. Political Analysis, 31(3), 337–351.

Asvadi, A., Premebida, C., Peixoto, P., & Nunes, U. [2016]. *3D Lidarbased static and moving obstacle detection in driving environments.* Robotics and Autonomous Systems, 83, 299–311.

Gershman, S. J., & Daw, N. D. [2017]. *Reinforcement learning and episodic memory in humans and animal.* Annual Review of Psychology, 68, 101–128.

Hägerstrand, T. [1970]. What about people in regional science? *Papers in Regional Science*, 24(1), 7–24.

He, Q., Liu, J. L., Eschapasse, L., Beveridge, E. H., & Brown, T. I. [2022]. *A comparison of reinforcement learning models of human spatial navigation.* Scientific Reports, 12, 13923.

Kwan, M. P., & Schwanen, T. [2016]. *Geographies of mobility.* Annals of the American Association of Geographers, 106(2), 243–256.

Liao, F., Tian, Q., Arentze, T., Huang, H.-J., & Timmermans, H. J. P. [2020]. Travel preferences of multimodal transport systems in emerging markets. *Transportation Research Part A: Policy and Practice*, 138, 250–266.

Miller, H. J. [1991]. *Modelling accessibility using space-time prism concepts within geographical information systems.* International Journal of Geographical Information Systems, 5(3), 287–301.

Tokey, A. I., Liu, L., & Miller, H. J. [2025]. *Measuring the impacts of sidewalks on public transit first-mile/last-mile accessibility and their association with social and demographic factors*. Transportation Research Interdisciplinary Perspectives, 33, 101576.

Tong, Y., & Bode, N. W. F. [2022]. *The principles of pedestrian route choice.* Journal of the Royal Society Interface, 19(189), 20220061.

Udhayasekar, S., Srinivasan, K., & Chilukuri, B. [2026]. *Revisiting transit accessibility: effect of stochasticity, real-time information, congestion, and network structure.* Journal of Engineering and Applied Science, 73, 35.

Zhang, H., Deng, H., Ou, J., & Feng, C. [2025]. *Mitigating spatial hallucination in large language models for path planning via prompt engineering.* Scientific Reports, 15, 8881.

APPENDIX A

Figure A1

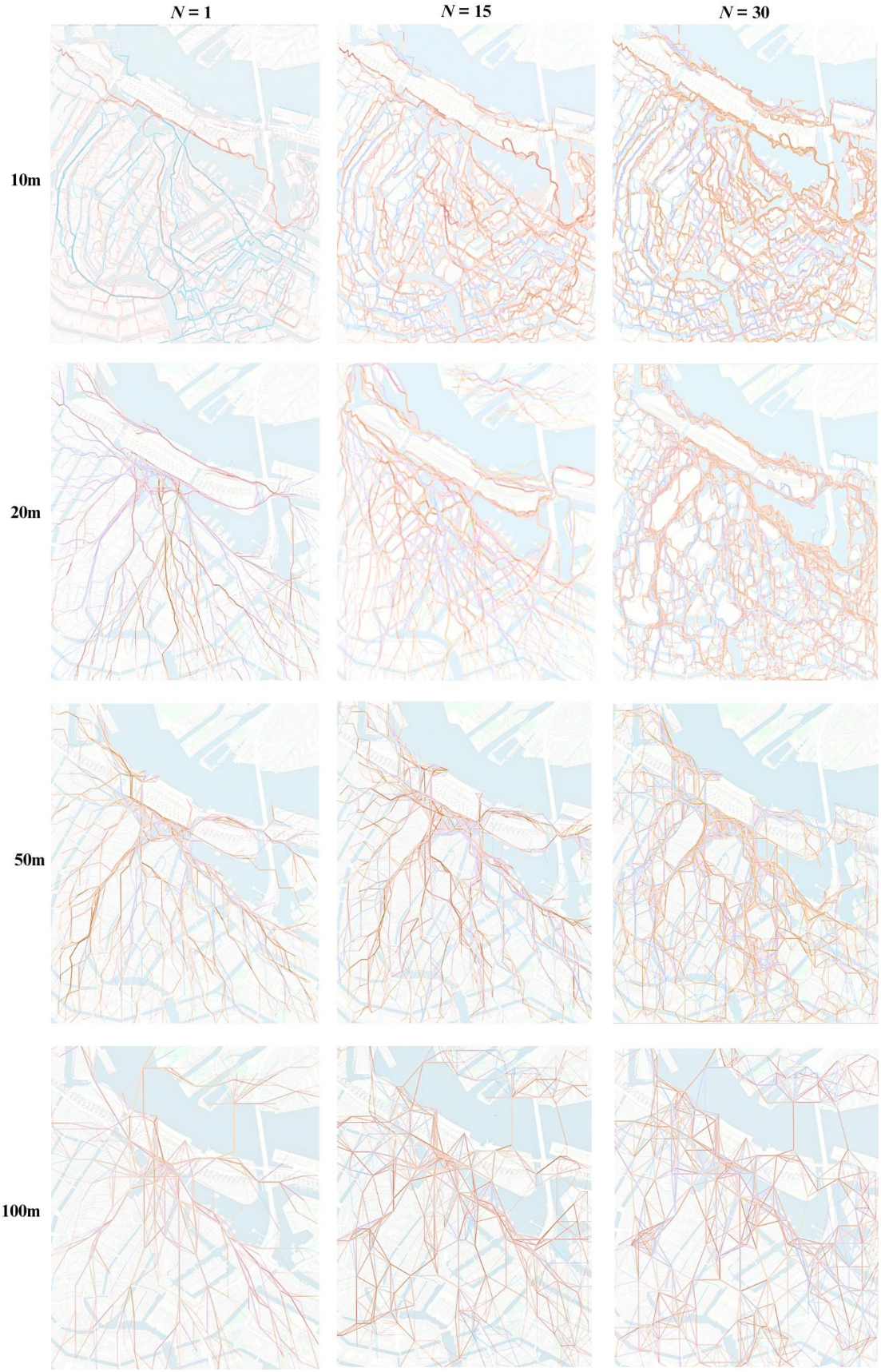


Figure A2

